SCATTERING CHARACTERISTICS OF PHOTON DENSITY WAVES FROM AN OBJECT EMBEDDED IN A SPHERICALLY TWO-LAYER TURBID MEDIUM

Yuqi Yao and Yao Wang
Department of Electrical Engineering
Polytechnic University, Brooklyn, NY 11201

Randall L. Barbour, Harry L. Graber and Jenghwa Chang
Department of Pathology and Biophysics
SUNY Health Science Center, Brooklyn, NY 11203

ABSTRACT

We present an analytic solution to the amplitude and phase distributions of photon density waves in strongly scattering, spherically symmetric, two-layer media containing a spherical object. The normal mode series method is employed to solve the inhomogeneous Helmholtz equation in spherical coordinates, with suitable boundary conditions. By comparing the total field on the surface of the outer layer when the object is present to when it is absent, we evaluate the potential sensitivity of an optical imaging system to inhomogeneities in absorption and scattering. For four types of background media which are different in their absorption and scattering properties, we determine: i) the modulation frequency that achieves an optimal compromise between signal detection reliability and sensitivity to the presence of object; ii) the minimum detectable object radius; iii) the smallest detectable change in its absorption coefficient and iv) scattering coefficient for a fixed object size. A discussion of the qualitative and quantitative findings is given.

1. INTRODUCTION

Recently, it has been shown that the propagation of light emitted from a sinusoidally varying intensity–modulated source in a strongly scattering medium is governed by the scalar Helmholtz wave equation. Such a wave is referred to as a photon density wave (PDW) [1,2] or diffuse photon density wave (DPDW) [3]. The former starts from the diffusion approximation to the Boltzmann transport equation; the latter uses the diffusion equation. Based on this result, light propagation can be analyzed in the frequency domain using theories and methodologies developed for electromagnetic (EM) and acoustic waves. The major difference between PDW and EM or acoustic waves is that the wavenumber k of the PDW, which depends on the optical properties as well as on the modulation frequency, has a large imaginary part. Physically, this implies an exponential attenuation of the wave's amplitude as the wave propagates away from the source, even for a nonabsorbing medium. Some important phenomena have been investigated, including the propagation [2], diffraction and reflection [1,3], and scattering [4,5] of PDW and image reconstruction [6].

Imaging requires solution to the inverse scattering problem (ISP). In the inverse scattering problem, the goal is to derive the optical properties of the test medium from the measured scattered field on the surface of the medium. So far, investigations of the direct problem and ISP have been mostly limited to the case of an object embedded within an otherwise homogeneous infinite medium. In the present work, we study scattering from a spherical object embedded in the center of an infinite, two-layer spherically symmetric background medium. Each layer is assigned optical properties in the range typical of most tissue types. The object is different from the surrounding layers in its absorption or scattering coefficient or both. Here, we consider only the case of an object located at the center of the inner layer so that the test medium is in fact a spherically-symmetric, three-layer medium. An analytic solution for the total field

0-8194-1736-X/95/$6.00

in this piecewise homogeneous structure, due to a source located on a spherical surface in the outer layer, is derived by using the normal mode series (NMS) method with appropriate boundary conditions. For a given set of background medium properties, this solution is then used to derive the total field on the same surface in the outer layer for various modulation frequencies, object sizes and object optical properties. Four types of background media are examined: Type I – the outer layer is more absorbing, both layers equally scattering; Type II – the outer layer is less absorbing, both layers equally scattering; Type III – the outer layer is more scattering, both layers equally absorbing; Type IV – the outer layer is less scattering, both layers equally absorbing. In addition to identifying limits on detectability, we report several new findings that may prove useful in evaluating methods for imaging dense scattering media.

2. PROBLEM FORMULATION AND SOLUTION

We consider a spherical inhomogeneity (object) embedded in a spherically symmetric, two-layer background medium. The geometry of this general three-layer structure is shown in Fig. 1. The radii of the object, the inner layer, and the measurement surface of the outer layer are denoted by a, b and c, respectively. In the reported studies, the radius of the inner layer is fixed at $b = 3$ cm. The absorption and reduced scattering coefficient are denoted by μ_{ai} and μ'_{si}, respectively, for Ω_i. Here, Ω_1 refers to $r > b$ (*i.e.*, outer layer), Ω_2 for $a < r < b$ (*i.e.*, inner layer) and Ω_3 for $0 \leq r < a$ (*i.e.*, object). We adopt a spherical coordinate system with origin at the center of the inner sphere. The problem is to determine the total field at various points on a surface in the outer layer, $\mathbf{r} = (r, \theta, \phi), r = c$, due to a sinusoidally varying intensity-modulated point source of light placed at a point on the same surface $\mathbf{r}' = (r', \theta', \phi'), r' = c$. In our study, the radius of the measurement surface is fixed at c= 4 cm.

Let $G(\mathbf{r}, \mathbf{r}')$ represent the photon density at $\mathbf{r}$ due to a unit strength point source at $\mathbf{r}'$. Then $G(\mathbf{r}, \mathbf{r}')$ is the Green's function for the following non-homogeneous Helmholtz wave equation [1,7]:

$$\nabla^2 G_j(\mathbf{r}, \mathbf{r}') + k_j^2 G_j(\mathbf{r}, \mathbf{r}') = -\delta(\mathbf{r} - \mathbf{r}'); \quad \text{for } \mathbf{r} \in \Omega_j, \quad j = 1, 2, 3. \tag{1}$$

The squared complex wavenumber is given by

$$k_j^2 = -\frac{\mu_{aj}}{D_j} + i\frac{\omega}{v_j D_j}, \quad \text{with} \begin{cases} \omega = 0, & \text{for DC} \\ \omega \neq 0, & \text{for AC} \end{cases} \tag{2}$$

where v_j is the speed of a photon in Ω_j, and $D_j = 1/3(\mu_{aj} + \mu'_{sj})$, is the diffusion coefficient.

The total field in the outer layer can, in general, be interpreted as a superposition of the incident spherical wave G_i plus a scattering spherical wave G_{s1}, *i.e.*:

$$G_1(\mathbf{r}, \mathbf{r}') = G_i(\mathbf{r}, \mathbf{r}') + G_{s1}(\mathbf{r}, \mathbf{r}'), \tag{3}$$

$$G_i(\mathbf{r}, \mathbf{r}') = \frac{ik_1}{4\pi} \sum_{n=0}^{\infty} \sum_{m=0}^{n} (2 - \delta_m)(2n+1)\frac{(n-m)!}{(n+m)!} \cdot h_n^{(1)}(k_1 r') j_n(k_1 r) P_n^m(\cos\theta) P_n^m(\cos\theta') \cos m(\phi - \phi'), \tag{4}$$

$$G_{s1}(\mathbf{r}, \mathbf{r}') = \frac{ik_1}{4\pi} \sum_{n=0}^{\infty} \sum_{m=0}^{n} A_{mn}(2 - \delta_m)(2n+1)\frac{(n-m)!}{(n+m)!} \cdot h_n^{(1)}(k_1 r') h_n^{(1)}(k_1 r) P_n^m(\cos\theta) P_n^m(\cos\theta') \cos m(\phi - \phi'). \tag{5}$$

Similarly, the total field in the inner layer can be represented as the sum of a transmitted spherical wave and a scattering field, *i.e.:*

$$G_2(\mathbf{r},\mathbf{r}') = G_{t2}(\mathbf{r},\mathbf{r}') + G_{s2}(\mathbf{r},\mathbf{r}'), \tag{6}$$

$$G_{t2}(\mathbf{r},\mathbf{r}') = \frac{ik_1}{4\pi}\sum_{n=0}^{\infty}\sum_{m=0}^{n} B_{mn}(2-\delta_m)(2n+1)\frac{(n-m)!}{(n+m)!}$$
$$\cdot h_n^{(1)}(k_1 r')j_n(k_2 r)P_n^m(\cos\theta)P_n^m(\cos\theta')\cos m(\phi-\phi'), \tag{7}$$

$$G_{s2}(\mathbf{r},\mathbf{r}') = \frac{ik_1}{4\pi}\sum_{n=0}^{\infty}\sum_{m=0}^{n} C_{mn}(2-\delta_m)(2n+1)\frac{(n-m)!}{(n+m)!}$$
$$\cdot h_n^{(1)}(k_1 r')y_n(k_2 r)P_n^m(\cos\theta)P_n^m(\cos\theta')\cos m(\phi-\phi'). \tag{8}$$

The field in the object consists of a transmitted spherical wave, *i.e.:*

$$G_3(\mathbf{r},\mathbf{r}') = \frac{ik_1}{4\pi}\sum_{n=0}^{\infty}\sum_{m=0}^{n} D_{mn}(2-\delta_m)(2n+1)\frac{(n-m)!}{(n+m)!}$$
$$\cdot h_n^{(1)}(k_1 r')j_n(k_3 r)P_n^m(\cos\theta)P_n^m(\cos\theta')\cos m(\phi-\phi'). \tag{9}$$

In the previous equations, j_n, y_n, and $h_n^{(1)}$ are the spherical Bessel function, Neuman function, and the Hankel function of the first kind, respectively, and P_n^m is the associated Legendre function [9], $\delta_m = 1, m = 0; 2, m \geq 1$.

The unknown expansion coefficients, A_{mn}, B_{mn}, C_{mn} and D_{mn}, in the above equations can be determined by subjecting the total fields G_i, i=1,2,3, to the following boundary conditions [8]: (i) The photon density, G, is continuous at $r = b$ and $r = a$; (ii) The photon current, $\mathbf{J}$, is continuous at $r = b$ and $r = a$; (iii) G is bounded at $r = 0$ and satisfies a radiation condition at $r \to \infty$.

The resulting coefficients A_{mn} in Eq.(4) are the ratios of two 4×4 determinants as follows [10,11]:

$$A_{mn} = \begin{vmatrix} A_1^* & a_{12} & a_{13} & 0 \\ A_2^* & a_{22} & a_{23} & 0 \\ 0 & a_{32} & a_{33} & a_{34} \\ 0 & a_{42} & a_{43} & a_{44} \end{vmatrix} \Bigg\| \begin{vmatrix} a_{11} & a_{12} & a_{13} & 0 \\ a_{21} & a_{22} & a_{23} & 0 \\ 0 & a_{32} & a_{33} & a_{34} \\ 0 & a_{42} & a_{43} & a_{44} \end{vmatrix}^{-1} \tag{10}$$

where $A_1^* = k_1 D_1 j_n'(k_1 b)$, $A_2^* = k_1 D_1 j_n(k_1 b)$, $a_{11} = k_1 D_1 h_n^{(1)'}(k_1 b)$, $a_{12} = k_2 D_2 y_n'(k_2 b)$, $a_{13} = k_2 D_2 j_n'(k_2 b)$, $a_{21} = k_1 D_1 h_n^{(1)}(k_1 b)$, $a_{22} = y_n(k_2 b)$, $a_{23} = j_n(k_2 b)$, $a_{32} = y_n(k_2 a)$, $a_{33} = j_n(k_2 a)$, $a_{34} = j_n(k_3 a)$, $a_{42} = k_2 D_2 y_n'(k_2 a)$, $a_{43} = k_2 D_2 j_n'(k_2 a)$ and $a_{44} = k_3 D_3 j_n'(k_3 a)$.

In this paper, we use $|G_t|$ and Φ_t to represent the magnitude and phase of the total field when the object is present, and use $|G_b|$ and Φ_b for the case when the object is absent (*i.e.,* the background medium). The total field for the background medium is referred to as the *background field.* The difference between the total field and the background field in the presence of an object is the scattered field from the object. The background field here plays the role of the incident field when one studies the scattering due to an object embedded in an otherwise homogeneous background. In the following, we measure the sensitivity of a detector to a hidden object by the *relative amplitude change* δ_G and *phase-change* δ_Φ. These are defined as, respectively,

$$\delta_G = 1 - \frac{|G_t|}{|G_b|}, \tag{11}$$

and

$$\delta_\Phi = \Phi_b - \Phi_t. \tag{12}$$

The optical properties of the outer layer of the four different background media are $\mu_{a_1} = 0.08\text{cm}^{-1}$ and $\mu'_{s_1} = 10.0\text{cm}^{-1}$ for Type I; $\mu_{a_1} = 0.02\text{cm}^{-1}$ and $\mu'_{s_1} = 10.0\text{cm}^{-1}$ for Type II; $\mu_{a_1} = 0.04\text{cm}^{-1}$ and $\mu'_{s_1} = 20.0\text{cm}^{-1}$ for Type III, $\mu_{a_1} = 0.04\text{cm}^{-1}$ and $\mu'_{s_1} = 5.0\text{cm}^{-1}$ for Type IV, respectively. The absorption and scattering coefficients of the inner layer are fixed at $\mu_{a_2} = 0.04\text{cm}^{-1}$ and $\mu'_{s_2} = 10.0\text{cm}^{-1}$. For each background medium, we introduce an object in the inner layer and vary its radius, absorption and scattering properties. For each background medium, we seek to answer four questions: i) at which modulation frequency f, is the amplitude $|G_b|$ of the background field large enough to be measured reliably while the changes δ_G and δ_Φ due to the presence of an object are detectable as defined below? Based on this study, we select a modulation frequency for use in studying the following three problems. ii) For a fixed modulation frequency and object optical properties, what is the radius, $a_{\min}$, of the smallest detectable object? iii) For a fixed modulation frequency and a fixed object size, what is the smallest relative change in absorption, $\delta_{a,\min} = (\mu_{a_3} - \mu_{a_2})/\mu_{a_2}$, that can be detected? iv) Similarly, what is the smallest relative change in scattering, $\delta_{s,\min} = (\mu'_{s_3} - \mu'_{s_2})/\mu'_{s_2}$, that can be detected? In answering these questions, we define a detectable signal as one for which the amplitude of the total field is no smaller than $|G_{\min}| = 10^{-10}$ and the relative change in amplitude and absolute change in phase must be greater than or equal to $\delta_{G,\min} = 0.1\%$ and $\delta_{\Phi,\min} = 0.1°$, respectively. Combining the requirement for $|G_{\min}|$ and $\delta_{G,\min}$, the amplitude of the background field should be at least $|G_{b,\min}| = 10^{-7}$.

3. RESULTS

3.1 Influence of Modulation Frequency

In order to determine the optimal modulation frequency for different background media, we have evaluated the amplitude and phase of the total field with and without the object present for several frequencies: $f = 0$ (DC), 100, 200, and 500 MHz. Fig. 2 shows the amplitude distribution of the background field at these frequencies. As expected, the amplitude of the background field is reduced for increasing detector angles at a fixed frequency, or for increasing frequencies at a fixed detector angle. The background field of Type I and type III are approximately 10-100 fold smaller than Type II and Type IV respectively because of the stronger absorption or scattering in the outer layer. Figs. 3 and 4 show the relative amplitude change and absolute phase change due to an object. We observe that at larger detector angles, expect for Type I medium, the amplitude changes increase with the modulation frequencies and the DC component has the lowest amplitude sensitivity. Interestingly, nearly the opposite trend is seen with Type I medium. On the other hand, for all four types of background media, the phase sensitivity increases with the frequency.

Comparison of these data show that when a gradient in the absorption coefficient exists (i.e., for Type I and Type II), a peak in the phase plot is seen at an intermediate detector angle, $130° - 145°$ for Type I background media and $125° - 140°$ for Type II background media. The amplitude and position of this peak vary with the modulation frequency, with higher positive values observed for higher frequencies. For Type II media we also observed that at detector angles $> 130°$, the algebraic sign of the phase change becomes negative, and is a function of the modulation frequency. A qualitatively different trend is observed for background media having a gradient in scattering (*i.e.*, Type III and IV). Little to no intermediate peak is seen and, at larger detector angles and higher modulation frequencies, the phase changes seen have an increasingly more negative value.

Based on the criteria that the amplitude of the background filed should be greater than $|G_{b,\min}| = 10^{-7}$, the optimal modulation frequencies which achieve the best compromise between signal strength and relative response are approximately 200, 300, 200 and 500 MHz. For comparison purposes, however, we select a frequency of 200 MHz for all the background media in the following studies.

3.2 Effect of Variations in Absorption Coefficient of the Object

Results in Figs. 5 and 6 show the computed sensitivities to a change in the absorption coefficient of the object as a function of detector angle for each of the background media tested. For these studies the size of the object and its scattering coefficient are fixed at $a = 0.5$ cm and 10cm^{-1}, respectively. In each case, the absorption coefficient of the object was varied over a range of approximately $0.04 - 0.1\text{cm}^{-1}$. At increasing detector angles and absorption values, the change in amplitude increases monotonically in a nonlinear fashion. Fig. 6 shows that a perturbation in absorption produces a peak in the phase plot at an intermediate detector angle ($120° - 140°$). The amplitude and position of this peak vary with the value of the absorption coefficient of the object, with higher positive values observed for larger values of μ_a. For Type II media we also observe that at detector angles $> 140°$, the algebraic sign of the phase change becomes negative, and is a function of μ_a. Further inspection shows, interestingly, the existence of an "isosbestic" point at $\theta \approx 145°$, indicating that at this angle the detector is insensitive to a change in the absorption coefficient of the object. A quantitative comparison of the phase shift and relative changes in amplitude for the different media reveals greater sensitivity to perturbations in absorption in the object for Type I and III media. By interpolating the data in these plots, we determine that the smallest detectable perturbation in absorption varies from approximately 0.0015 to 0.005cm^{-1} ($3.75 - 12.5\%$) for amplitude data and 0.01 to 0.02cm^{-1} ($25 - 50\%$) for phase data, depending on the properties of the background medium. See Table 1.

3.3 Effect of Variations in Scattering Coefficient of the Object

Results in Figs. 7 and 8 show the computed responses of the effect that a change in the scattering coefficient of the object has on the relative change in the amplitude and phase change as a function of detector angle for each of the background media tested. Note that for these studies the size of the object and its absorption coefficient are fixed at $a = 0.5$ cm and 0.04 cm^{-1}, respectively. In each case the scattering coefficient of the object was varied over a range of approximately $10 - 20\text{cm}^{-1}$. A qualitative examination of the amplitude and phase plots reveals little difference in the responses seen for different media. In all cases, an increase in the scattering coefficient of the object produces a nonlinear, monotonic increase in the relative change of amplitude, with larger differences seen at larger detector angles. A qualitatively similar response is seen in the phase data. In this case, the phase change becomes increasingly more negative at larger detector angles and for larger values of the scattering coefficients. By linearly interpolating the data for other intermediate values for the scattering coefficient, we have found that the smallest detectable change, $\delta_{s,\text{min}}$, varies from 0.2 to 0.45cm^{-1} ($2 - 4.5\%$) based on amplitude measurements and 0.4 to 0.8cm^{-1} ($4 - 8\%$) for phase measurements at $\theta = 180°$. See Table 1.

A comparison of the responses in the phase and amplitude data produced by a perturbation in absorption (Figs. 5 and 6) to a perturbation in scattering (Figs. 7 and 8) show important qualitative and quantitative differences. Qualitatively, we observe that unlike the trends seen in the amplitude data, the phase data show distinctly different responses to a perturbation in the absorption and scattering coefficients. A quantitative comparison reveals that amplitude measurements are proportionally more sensitive to a change in absorption while phase measurements are proportionally more sensitive to a change in scattering. In absolute terms, however, we observed that in all cases amplitude measurements are more sensitive than phase measurements. A further inspection reveals that the trend seen in the phase data can be further influenced by differences in the optical properties of the outer layer. A comparison of phase data obtained from Type I and Type III media shows that a perturbation in absorption in the object causes a greater phase change for Type I medium while the opposite trend is seen for a perturbation in scattering.

3.4 Effect of Variations in Object Diameter

Results in Figs. 9 and 10 show the computed sensitivities to a change in the object size as a function of detector angle for each of the background media tested. For these studies, the absorption and scattering coefficients of the object are fixed; for Type I and II media, $\mu_{a_3} = 0.06\text{cm}^{-1}$, $\mu'_{s_3} = 10.0\text{cm}^{-1}$; for Type III and IV media, $\mu_{a_3} = 0.04\text{cm}^{-1}$, $\mu'_{s_3} = 15.0\text{cm}^{-1}$. Thus, for a specified object size, only a perturbation in absorption and only a perturbation in scattering exists for Type I and II media and Type III and IV media, respectively. The radius of the object was varied from approximately 0.2 to 1.0 cm. Similar to the trends seen for the other perturbations, inspection of the amplitude data reveals little to no qualitative differences in the responses seen for the different media. At increasing detector angles and object size, the change in amplitude increases monotonically in a nonlinear fashion. A similar comparison for the phase data, however, shows a qualitatively different response. For Type I and II media, a perturbation in object size produces a peak in the phase plot at an intermediate detector angle, $120° - 140°$. The amplitude and position of this peak varies with object size with higher positive values observed for larger radii. In fact, the responses seen for both the amplitude and phase data for Type I and II media to a perturbation in object size appear qualitatively, almost indistiguishable from those produced by a perturbation in the absorption coefficient (see Figs. 5 and 6). A qualitatively similar response is observed for Type III and IV media with respect to the changes seen in the amplitude and phase plots for a perturbation in scattering (see Figs. 7 and 8). Interestingly, we also observe in the phase data an "isosbestic" point at $\theta \approx 145°$ for Type II media. This finding demonstrates that under the specified conditions, the detector is insensitive to variations in object size. Interpolation of the plotted data shows that the smallest detectable perturbation in object radii varies from approximately 0.2 to 0.25 cm for amplitude data and 0.23 to 0.5 cm for phase data, depending on the properties of the background medium. See Table 1.

4. DISCUSSION AND CONCLUSION

We have derived an analytic solution for the PDW in a spherically symmetric, two-layer, highly scattering, infinite medium containing a spherical object. The changes in the amplitude and phase shift of the total field caused by the object have been calculated as functions of the modulation frequency, the object radius and the differences between the absorption and scattering coefficients of the object and the background. For each of four different types of background media, we have derived the optimal modulation frequency, the smallest detectable object size, and the minimal detectable differences in absorption and scattering coefficients. These results are summarized in Table 1. The quantitative results are based on certain assumptions about the precision of commercially available optical detectors. For a different set of detector precisions, one can easily derive corresponding results from the plots presented in Figs. 3-10. Comparing the corresponding figures for different background media, the following interesting points can be observed:

1. Whereas the absolute response of amplitude measurements are greater than phase measurements to changes in the absorption and scattering properties of an embedded object, the former are relatively insensitive to the type of perturbation. Phase measurements, on the other hand, exhibit a much greater differential response to perturbations in absorption and scattering.

2. Amplitude measurements are proportionally more sensitive to a change in absorption, while phase measurements are proportionally more sensitive to a change in scattering.

3. Enhanced sensitivity to an embedded object is achieved by an increase in the absorption or scattering properties of an outer layer.

4. Evidence of degenerate detector responses were observed under several conditions tested. This finding may make more difficult efforts to quantify the absolute optical coefficients of tissue by use of simplified measurement and analysis schemes.

5. REFERENCES

[1] J. Fishkin and E. Gratton, "Propagation of photon-density waves in strongly scattering media containing an absorbing semi-infinite plane bounded by a straight edge", *J. Opt. Soc. Am. A* 10, 127-140 (1993).

[2] B.J. Tromberg, L.O. Svaasand, T.T. Tsay and R.C. Haskell, "Properties of photon density waves in multiple-scattering media", *Applied Optics*, 32, pp. 607-616 (1993).

[3] M.A. O'Leary, D.A. Boas, B. Chance and A.G. Yodh, "Refraction of diffuse photon density waves", *Physical Review Letters*, 69, No.18, 2658-2661 (1992).

[4] D.A. Boas, M.A. O'Leary, B. Chance and A.G. Yodh, "Scattering of diffuse photon density waves by spherical inhomogeneities within turbid media: analytic solution and applications", *Proc. Natl. Acad. Sci. USA,* Vol. 91, pp. 4887-4891, (1994).

[5] A. Knuttel, J.M. Schmitt and J.R. Knutson, "Spatial localization of absorbing bodies by interfering diffusive photon-density waves ", *Applied Optics*, 32, No. 4, 381-389 (1993).

[6] M.A. O'Leary, D.A. Boas, B. Chance and A.G. Yodh, "Imaging of inhomogeneous turbid media using diffuse photon density waves", *In OSA Proceedings on Advances in Optical Imaging and Photon Migration*, R. R. Alfano, ed., pp. 106-115 (1994).

[7] A. Ishimaru, *Wave propagation and Scattering in Random media* (Academic Press, New York, 1978).

[8] J. J. Duderstadt and L. J. Hamilton, *Nuclear Reactor Analysis* (John Wiley & Sons, Inc., New York, 1976).

[9] M. Abramowitz and J. A. Stegun, *Handbook of Mathematical Functions* (Dover, New York, 1972).

[10] J.A. Stratton, *Electromagnetic Theory* (McGraw-Hill Book Company, Inc. New York, 1949).

[11] D.S. Jones, *Acoustic and Electromagnetic wave* (Clarendon Press, Oxford, New York, 1986).

ACKNOWLEDGEMENT

This work was supported in part by the National Institutes of Health under Grant # RO1-CA59955, by an ONR grant # N000149510063, and by the New York State Science and Technology Foundation.

Table 1: Optimal modulation frequency and minimal detectable object radius and absorption and scattering variation for different background media

Type	f_{opt} (MHz)	Detectable Signal Change	a_{min} (cm) ($\delta_a = 50\%$) ($f = 200$ MHz)		$\delta_{a,min}(\%)$ ($a = 0.5$ cm) ($f = 200$ MHz)		$\delta_{s,min}(\%)$ ($a = 0.5$ cm) ($f = 200$ MHz)	
I	200	$\delta_G \geq 0.1\%$	$\theta = 180°$	0.22	$\theta = 180°$	3.75	$\theta = 180°$	2.0
		$\delta_\Phi \geq 0.1°$	$\theta = 140°$	0.40	$\theta = 140°$	25.0	$\theta = 180°$	5.0
II	300	$\delta_G \geq 0.1\%$	$\theta = 180°$	0.25	$\theta = 180°$	5.0	$\theta = 180°$	4.0
		$\delta_\Phi \geq 0.1°$	$\theta = 180°$	0.50	$\theta = 180°$	50.0	$\theta = 180°$	4.0
III	200	$\delta_G \geq 0.1\%$	$\theta = 180°$	0.20	$\theta = 130°$	12.5	$\theta = 180°$	2.5
		$\delta_\Phi \geq 0.1°$	$\theta = 180°$	0.23	$\theta = 130°$	37.5	$\theta = 180°$	4.0
IV	500	$\delta_G \geq 0.1\%$	$\theta = 180°$	0.25	$\theta = 140°$	20.0	$\theta = 180°$	4.5
		$\delta_\Phi \geq 0.1°$	$\theta = 180°$	0.30	$\theta = 140°$	50.0	$\theta = 180°$	8.0

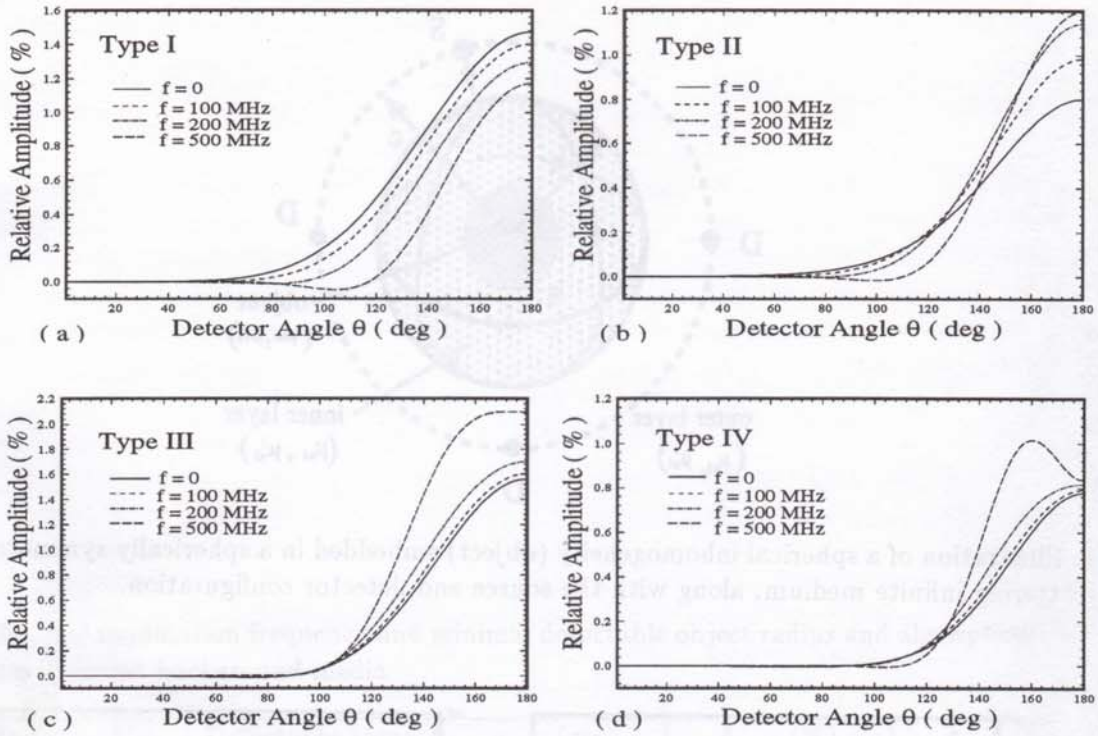

Figure 3: Percent change in amplitude versus detector angle for different modulation frequencies, due to a 0.5 cm radius object with $\mu_{a_3} = 0.06\text{cm}^{-1}$, $\mu'_{s_3} = 10.0\text{cm}^{-1}$ embedded in Type I, II background media and $\mu_{a_3} = 0.04\text{cm}^{-1}$, $\mu'_{s_3} = 15.0\text{cm}^{-1}$ embedded in Type III, IV background media.

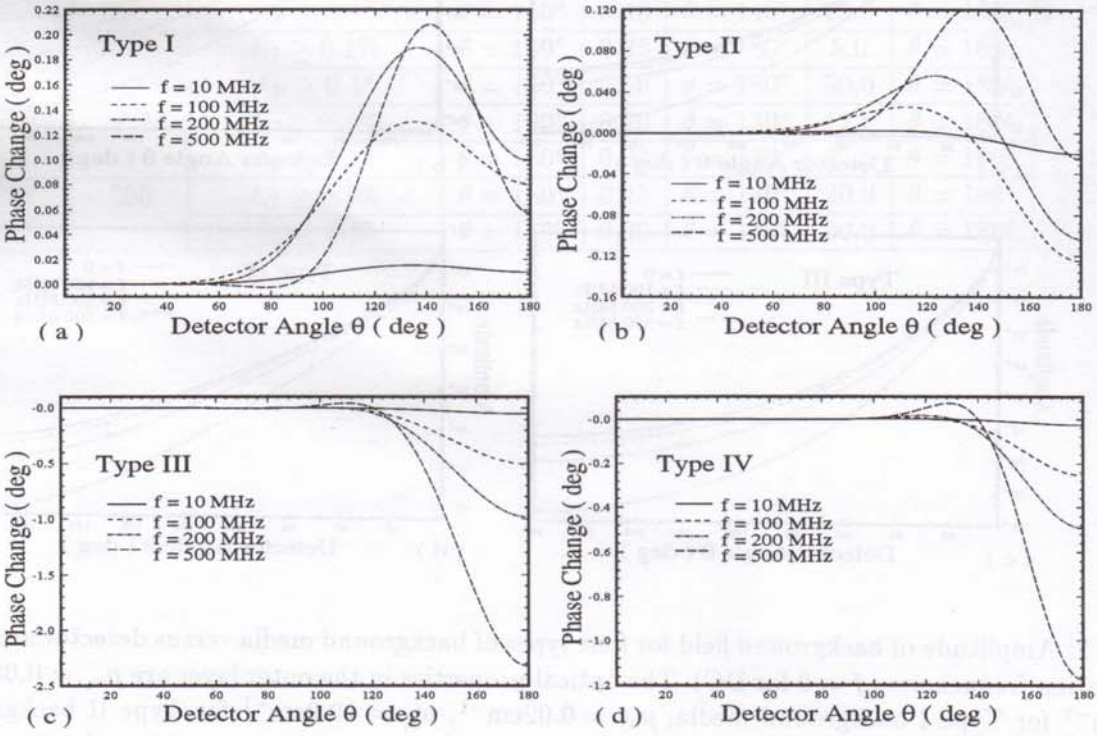

Figure 4: Phase change in degrees versus detector angle for different modulation frequencies, due to a 0.5 cm radius object with $\mu_{a_3} = 0.06\text{cm}^{-1}$, $\mu'_{s_3} = 10.0\text{cm}^{-1}$ embedded in Type I, II background media and $\mu_{a_3} = 0.04\text{cm}^{-1}$, $\mu'_{s_3} = 15.0\text{cm}^{-1}$ embedded in Type III, IV background media.

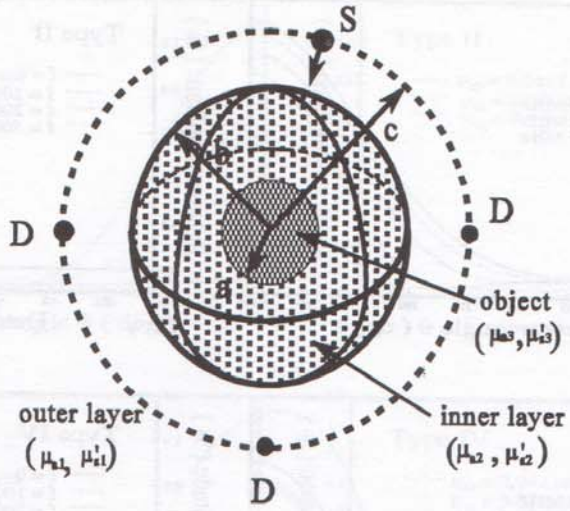

Figure 1: Illustration of a spherical inhomogeneity (object) embedded in a spherically symmetric two-layer, highly scattering infinite medium, along with the source and detector configuration.

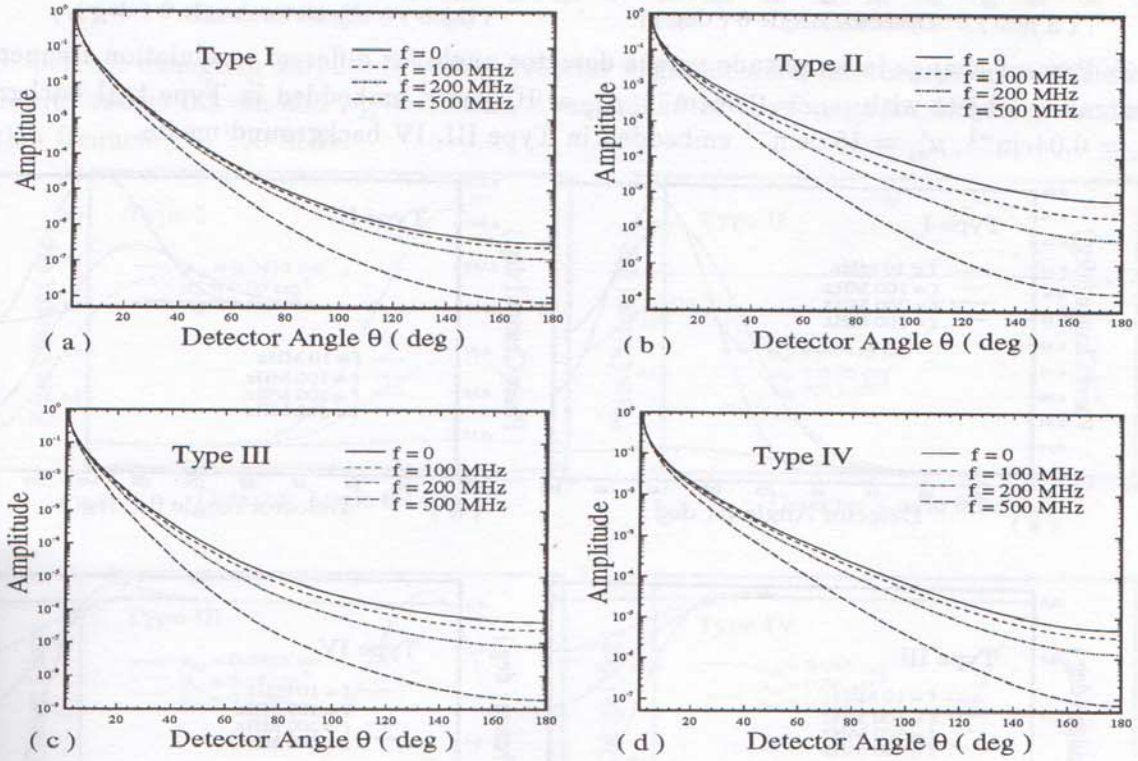

Figure 2: Amplitude of background field for four types of background media versus detector angle for several modulation frequencies ($f = 0$ for DC). The optical properties in the outer layer are $\mu_{a_1} = 0.08\text{cm}^{-1}$, $\mu'_{s_1} = 10.0\text{cm}^{-1}$ for Type I background media, $\mu_{a_1} = 0.02\text{cm}^{-1}$, $\mu'_{s_1} = 10.0\text{cm}^{-1}$ for Type II background media, $\mu_{a_1} = 0.04\text{cm}^{-1}$, $\mu'_{s_1} = 20.0\text{cm}^{-1}$ for Type III background media, and $\mu_{a_1} = 0.04\text{cm}^{-1}$, $\mu'_{s_1} = 5.0\text{cm}^{-1}$ for Type IV background media. The optical properties in the inner layer are the same for all four types of background media, being $\mu_{a_2} = 0.04\text{cm}^{-1}$ and $\mu'_{s_2} = 10.0\text{cm}^{-1}$.

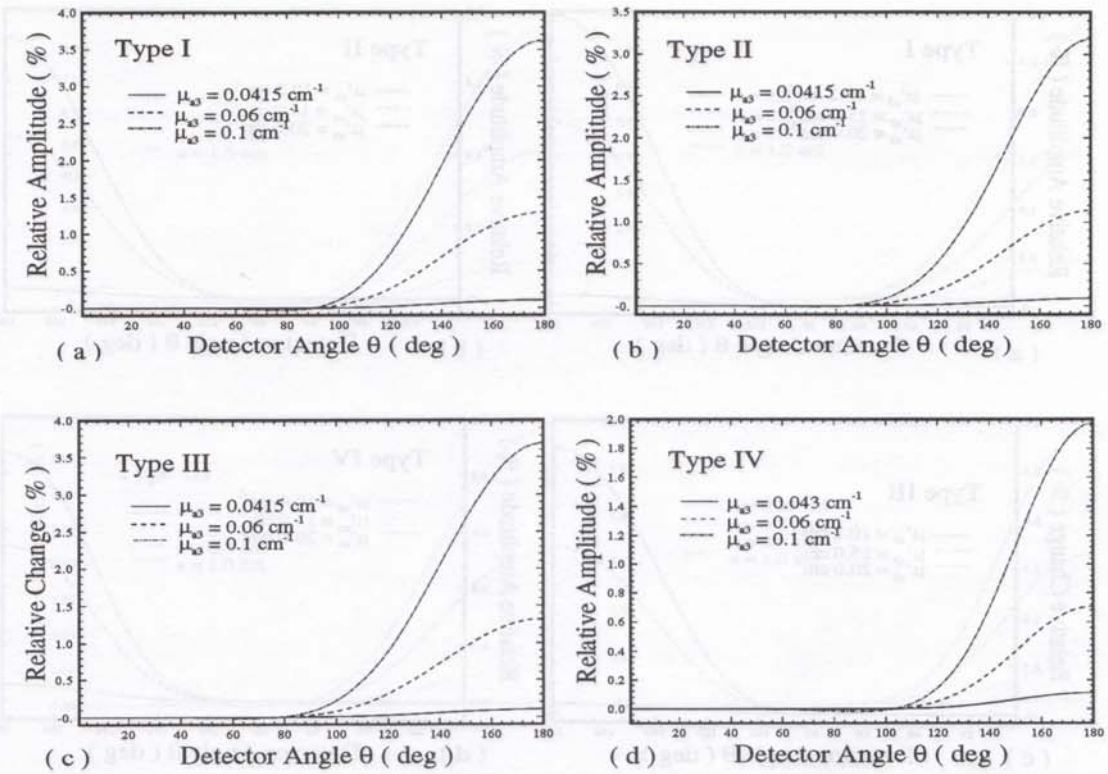

Figure 5: Percent change in amplitude versus detector angle for different absorption coefficients μ_{a_3} of an absorber with radius 0.5 cm and $\mu'_{s_3} = 10.0\text{cm}^{-1}$ embedded in the four types of background media. The modulation frequency is 200 MHz.

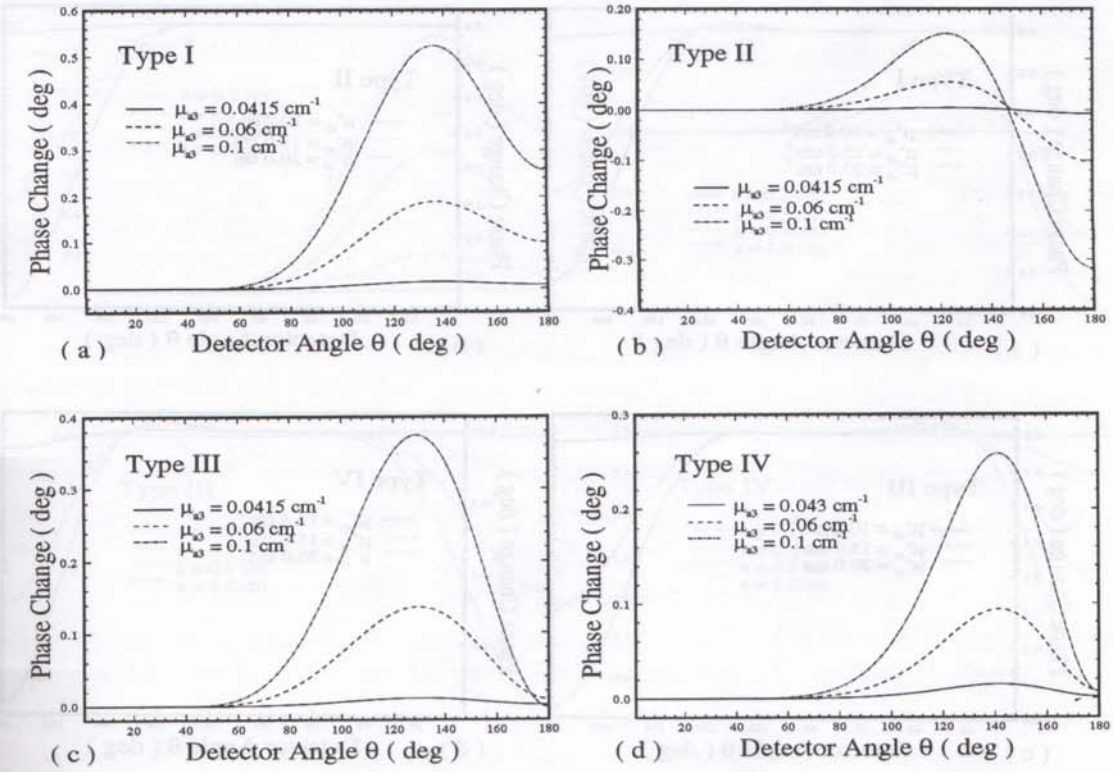

Figure 6: Phase change in degrees versus detector angle for different absorption coefficients μ_{a_3} of an object with radius 0.5 cm and $\mu'_{s_3} = 10.0\text{cm}^{-1}$ embedded in the four types of background media. The modulation frequency is 200 MHz.

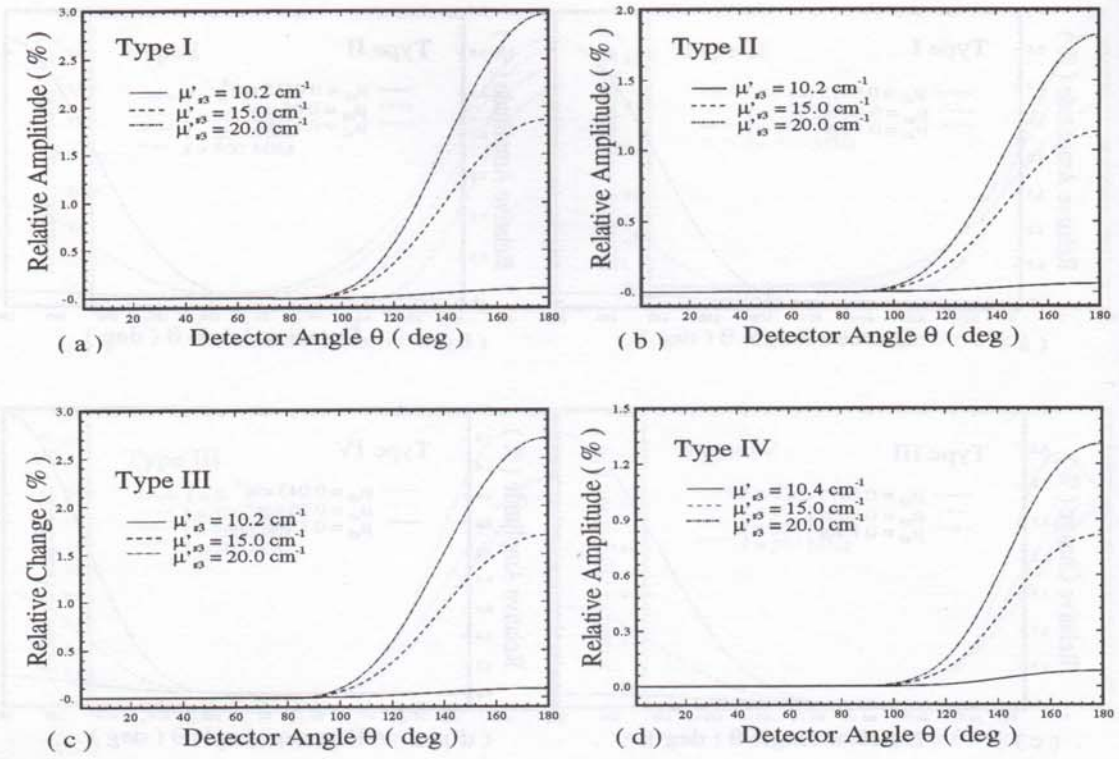

Figure 7: Percent change in amplitude versus detector angle for different scattering coefficients μ'_{s_3} of an absorber with radius 0.5 cm and $\mu_{a_3} = 0.04\text{cm}^{-1}$ embedded in the four types of background media. The modulation frequency is 200 MHz.

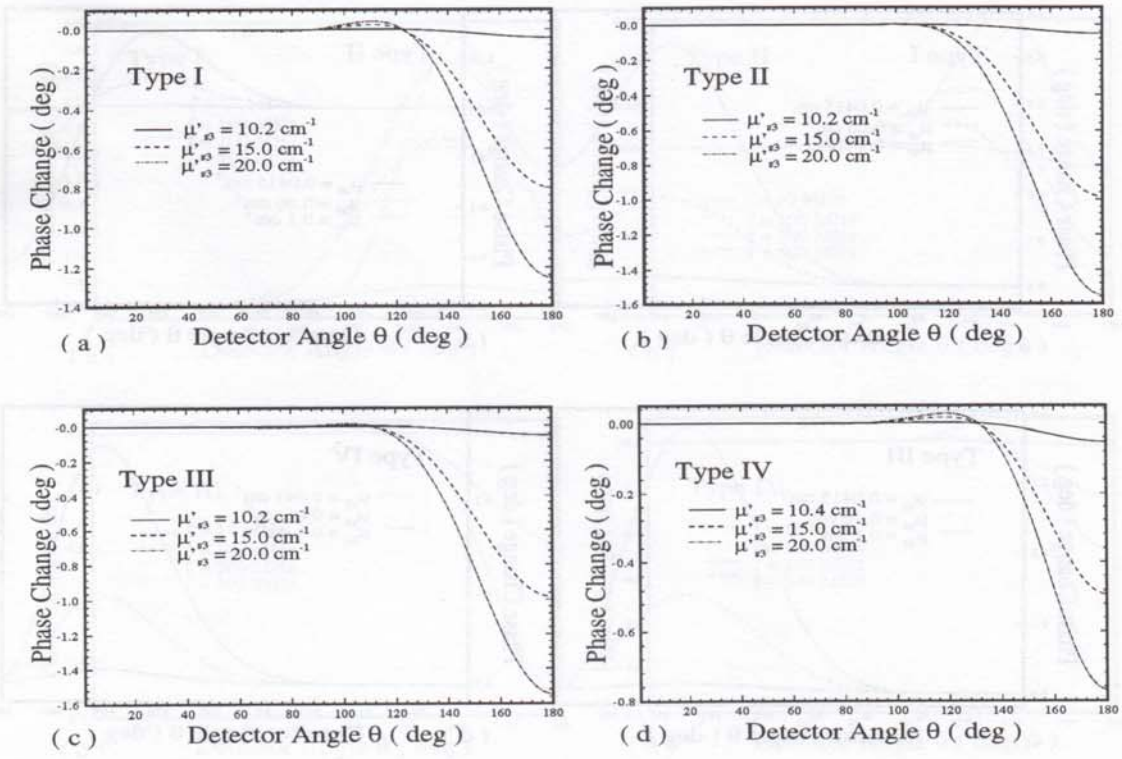

Figure 8: Phase change in degrees versus detector angle for different scattering coefficients μ'_{s_3} of an object with radius 0.5 cm and $\mu_{a_3} = 0.04\text{cm}^{-1}$ embedded in the four types of background media. The modulation frequency is 200 MHz.

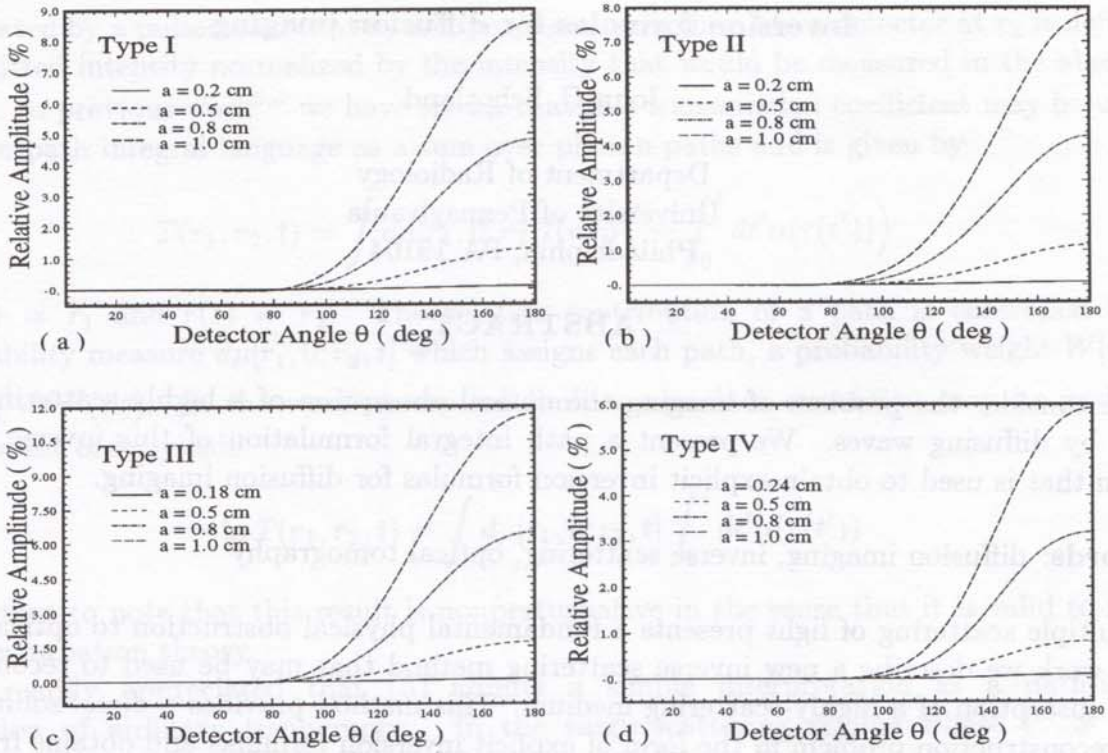

Figure 9: Percent change in amplitude versus detector angle for different radius a of the absorber with $\mu_{a_3} = 0.06\text{cm}^{-1}$, $\mu'_{s_3} = 10.0\text{cm}^{-1}$ embedded in Type I, II background media and $\mu_{a_3} = 0.04\text{cm}^{-1}$, $\mu'_{s_3} = 15.0\text{cm}^{-1}$ embedded in Type III, IV background media. The modulation frequency is 200 MHz.

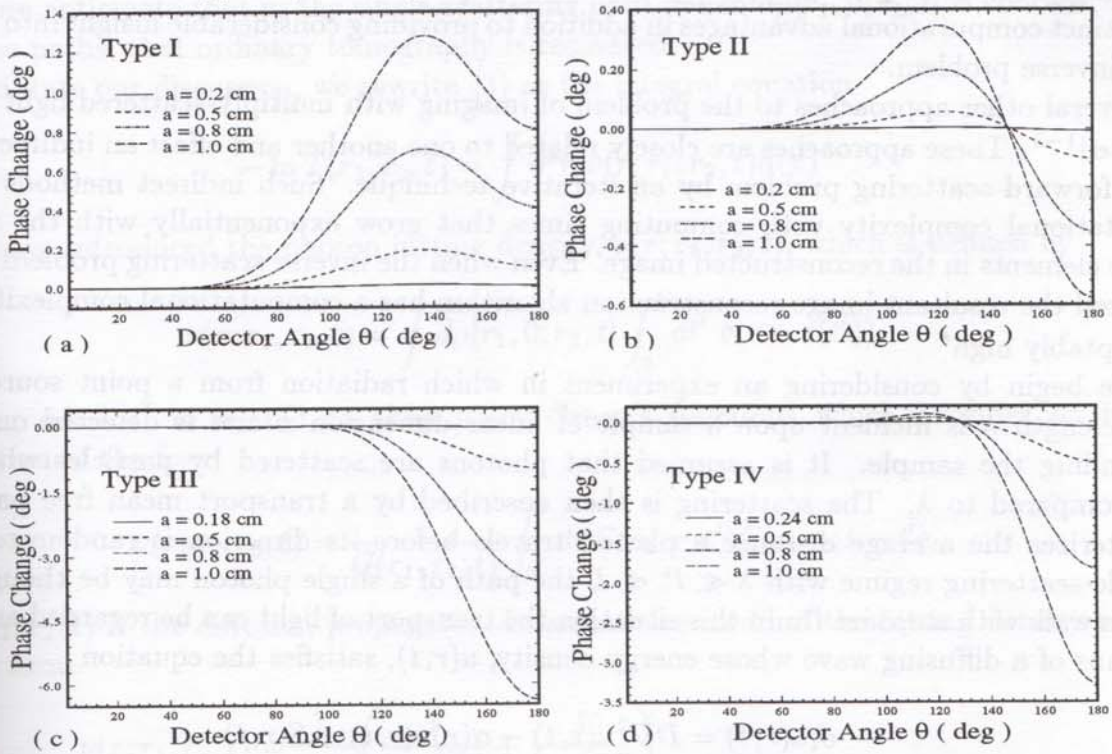

Figure 10: Phase change in degrees versus detector angle for different radius a of the absorber with $\mu_{a_3} = 0.06\text{cm}^{-1}$ and $\mu'_{s_3} = 10.0\text{cm}^{-1}$ embedded in Type I, II background media and $\mu_{a_3} = 0.04\text{cm}^{-1}$, $\mu'_{s_3} = 15.0\text{cm}^{-1}$ embedded in Type III, IV background media. The modulation frequency is 200 MHz.